IEEE Access
Multidisciplinary | Rapid Review | Open Access Journal

Received November 10, 2020, accepted December 1, 2020, date of publication December 4, 2020,
date of current version December 18, 2020.

Digital Object Identifier 10.1109/ACCESS.2020.3042572

An Improved Harmonic Suppression Control Strategy for the Hybrid Microgrid Bidirectional AC/DC Converter

GUISHUO WANG, (Fellow, IEEE), XIAOLI WANG, (Fellow, IEEE), AND JIECHAO LV
School of Mechanical, Electrical and Information Engineering, Shandong University, Weihai 264209, China
Corresponding author: Xiaoli Wang (wxl@sdu.edu.cn)

ABSTRACT The nonlinear load in AC/DC hybrid microgrid seriously affects the power transmission quality of bidirectional AC/DC interlinking converter (BIC). In this article, an improved Fryze-Buchholz-Depenbrock (FBD) harmonic current detection method combined with droop control is designed to suppress harmonic current control strategy. The decoupled double synchronous reference frame phase locked loop (DDSRF-PLL) with self decoupled network is used to eliminate the negative sequence fundamental frequency component, and the accurate phase detection can also be realized when affected by nonlinear load. The least mean square (LMS) algorithm adaptive filter can enhance the dynamic response ability when the load current suddenly changes. To solve the problem that the cut-off frequency of low pass filter (LPF) can not take into account the detection accuracy and response speed of FBD harmonic current detection method. Finally, Matlab/Simulink is used for simulation verification. The simulation results show that the improved control strategy not only realizes the bidirectional flow of power and maintains the DC bus voltage stability, but also reduces the total harmonic distortion (THD) at point of common coupling (PCC) by 0.45% compared with the traditional FBD control strategy. And the effectiveness and feasibility of the design method are proved.

INDEX TERMS AC/DC hybrid microgrid, bidirectional AC/DC interlinking converter, nonlinear load, improved FBD, droop control strategy, harmonic current suppression.

I. INTRODUCTION

In recent years, with the smart grid entering the comprehensive construction stage, an AC/DC hybrid microgrid system combines the advantages of both AC and DC microgrids has been widely studied [1]. A typic AC/DC hybrid microgrid is consists of AC sub-microgrid, DC sub-microgrid and bidirectional AC/DC converter. AC load and DC load can be connected to AC bus and DC bus respectively. This can greatly reduce the number of power electronic converter and reduce unnecessary power loss, which is considered to be the mainstream structure of the future microgrid [2], [3].

In grid-connected mode, the AC bus voltage and frequency are maintained by the public power grid because the AC sub-microgrid is connected to the public power grid. Therefore, the role of BIC is to maintain the voltage stability of DC sub-microgrid bus and control the power transmission between AC and DC sub-microgrids. When there are nonlinear loads in the systems, a seriously of harmonic currents and unbalanced load currents seriously affect the power quality transmitted by BIC. Therefore, the effective detection and compensation of harmonic current becomes particularly important. In literature [4], a harmonic current detection method based on instantaneous power theory ($i_p - i_q$ algorithm) is proposed. But $i_p - i_q$ algorithm involves complex matrix transformation, which requires a lot of work. In literature [5], proposed a harmonic detection method based on Fourier transform, which has high detection accuracy and can detection all harmonics. However, due to large amount of calculation and long delay time of detection, the real-time performance is poor. In literature [6], proposed an adaptive detection method, which not only considers the detection accuracy, but also ensure the response time. The detection accuracy is affected by the grid voltage amplitude. The FBD harmonic current detection method is proposed in literature [7], and the compensation current is calculated according

The associate editor coordinating the review of this manuscript and approving it for publication was Zhouyang Ren.

to the decomposition characteristics of equivalent conductance to current. Compared with $i_p - i_q$ method, it does not need complex matrix transformation, the detection effect is basically consistent, the calculation amount of is small, and the real-time performance is good. Based on the analysis of harmonic detection method, corresponding control method is needed to realize power transmission between AC and DC sub-microgrid.

Droop control is easy to realize the power balance between AC and DC sub-microgrids by simulating the frequency modulation characteristics of the generators, and has gradually become the mainstream of the control strategy of BIC. In literature [8], [9], the proposed AC frequency – active power ($f - P$) and AC voltage – reactive power ($u_{ac} - Q$) droop control strategies are not sensitive enough to load changes on DC side. In literature [10], a standardized control strategy is proposed, which compares the normalized treatment of DC bus voltage and AC frequency in the same coordinate system, so as to control the active power. The reactive power is controlled by the normalized AC bus voltage, and the characteristics between AC and DC sub-microgrid are fully considered. However, under the condition of grid connection, the voltage and frequency of AC bus are maintained by the public power grid and are basically maintained at the rated value. Therefore, the literature [11] proposed the DC voltage-active power ($u_{dc} - P$) droop control. However, when the DC bus voltage fluctuates near the rated value, the BIC will be frequency switched, resulting in loss. In literature [12], [13], a hierarchical droop control strategy is proposed to reduce the frequency switching of BIC.

The above droop control strategies are all control strategies under ideal conditions, and the situation of non-linear loads in microgrid is not analyzed. When the current is distorted by nonlinear load, it will cause additional power loss, interfere with grid-connected equipment, cause instability of microgrid system, and seriously affect power quality [14], [15]. In literature [16], a harmonic compensation strategy for low switching frequency of interconnected converters is proposed based on the virtual impedance theory. The harmonic compensation component is directly sent to the PWM reference signal, which reduces the influence of the closed-loop control bandwidth on the suppression of harmonic current to a certain extent. Its disadvantage is that the harmonic compensation accuracy is poor. In literature [17], presents a parallel operating transformer with a shared filter. This method has strong resonance damping ability, lower risk of resonance and better filtering performance. In literature [18], adding a proportional resonance controller to the BIC, which can effectively suppress the active and reactive power fluctuations and reduce the degree of current distortion. Its disadvantage is that it ignores the influence of negative sequence component of grid voltage, and the proportional resonance lacks ideal dynamic response performance. In literature [19], combined with active filtering method, proposed a controllable inductive power filtering (CIPF) method. It can effectively reduce the risk of harmonic resonance and greatly improve the performance of PWM rectifier. In literature [20], proposed a multi-mode control strategy for interlinking interface converters, which aims to deal with unbalanced power quality problems in a directional manner, and the scope of application is limited. In literature [21], [22], the proposed converter control strategy based on neural network and fuzzy control improves the accuracy of harmonic current suppression, with slow convergence speed and complex structure. In literature [23], a control strategy combining droop control with FBD harmonic detection method is designed, which can be well combined with the BIC structure. However, the limitations of traditional PLL and LPF limit the precision of control strategy to suppress harmonic current.

In view of the above analysis, this article adopts improved segmented droop control to avoid frequent switching of BIC due to voltage fluctuation of DC bus. The traditional FBD harmonic detection method is improved by DDSRF-PLL and LMS adaptive filter. This improved method can effectively solve the problems of the influence of negative sequence fundamental component, inaccurate phase lock when voltage and current distortion, and cut-off frequency of LPF can not take into account the accuracy and response speed of traditional FBD harmonic current detection method. By combining the improved FBD harmonic current detection method and droop control strategy, an improved FBD harmonic suppression droop control strategy is designed. When the nonlinear load causes the current distortion and generates the harmonic current, this method can not only suppress the harmonic current transmitted in the BIC, but also achieve bidirectional power flow and maintain the DC bus voltage stability under the non-ideal condition.

The rest of this article is shown below. Section 2 introduces the topology of AC/DC hybrid microgrid, the droop control strategy and topology of BIC. Section 3 introduces the harmonic current detection method, including the principle of FBD harmonic current detection method, DDSRF-PLL principle and adaptive filter based on LMS. Section 4 compares and verifies the improved method with the original method. Section 5 summarizes this whole article.

II. AC/DC HYBRID MICROGRID AND BIDIRECTIONAL AC/DC INTERLINKING CONVERTER

A. SYSTEM TOPOLOGY OF AC/DC HYBRID MICROGRID

At present, the topology of typical AC/DC hybrid microgrid is shown in Fig. 1 [24]. It consists of AC microgrid, DC microgrid, BIC and microgrid central controller. The AC/DC sub-microgrid contains various distributed generation units (DG), such as photovoltaic (PV), wind power (WTG), battery energy storage (ESS) and local loads.

Each distributed unit in the AC/DC sub-microgrid is connected to the AC and DC bus respectively through the converter. The AC and DC bus realizes the necessary power exchange and maintains system stability through the BIC. The AC/DC hybrid microgrid is connected to the public grid through PCC. The system operates in the grid-connected

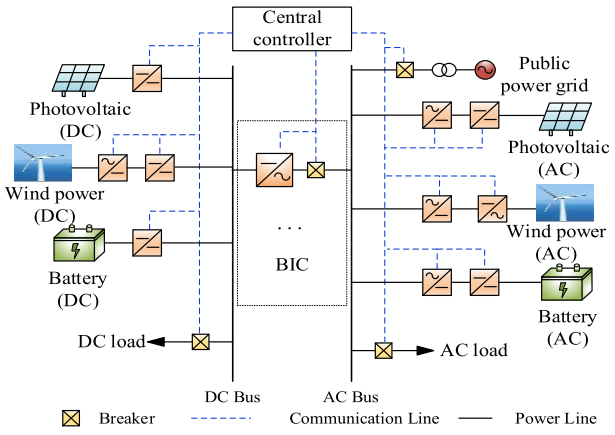

FIGURE 1. System topology of AC/DC hybrid microgrid.

mode, and the public grid is responsible for regulating the voltage and frequency stability of the AC sub-microgrid.

B. DROOP CONTROL STRATEGY FOR GRID-CONNECTED MODE

In the grid-connected mode, the public grid supports the voltage and frequency stability of the AC microgrid bus. The DG in the AC sub-microgrid can operate in MPPT mode. The energy storage device is in charging, discharging and standby state under unsaturated condition, and the excess energy in the microgrid system is feedback to the public grid [25]. Therefore, the main function of BIC is to ensure the power balance in the DC sub-microgrid, maintain the voltage stability of the DC bus, and realize the bidirectional flow of power.

Firstly, the active power droop control is introduced. In the grid-connected mode, the bus voltage and frequency of AC sub-microgrid are at rated value, so the BIC transmitted power is related to the DC bus voltage. The traditional ($P - U_{dc}$) droop characteristic curve formula can be described as:

$$u_{dc} = u_{dc}^{ref} - mP_{BIC}, \tag{1}$$

where, u_{dc} is the actual value of DC bus voltage, u_{dc}^{ref} is the reference value of DC bus voltage, m is the droop coefficient, and P_{BIC} is the active power transmitted by BIC. In order to protect the safe and stable operation of the BIC, when the voltage of the DC bus exceeds the maximum rated value, the active power transmitted by the BIC will be limited to the maximum of rated transmission power. At the same time, in order to avoid the small range fluctuation of BIC at the rated voltage of DC bus, resulting in frequent action of power switches tube and reducing unnecessary loss. Therefore, the $P - U_{dc}$ droop control was improved and the threshold value is set. The droop characteristic curve is shown in Figure 2.

According to the droop characteristic curve in Figure 2, the relationship between transmission active power and voltage

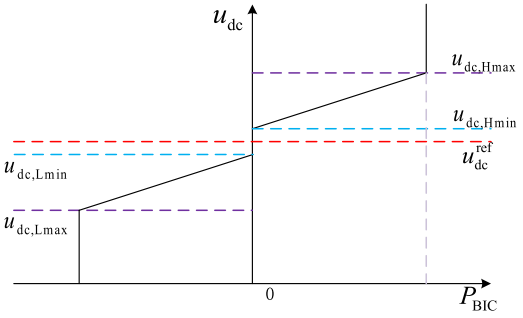

FIGURE 2. Improved $P - U_{dc}$ droop characteristic curve.

can be obtained, which can be expressed as:

$$P_{BIC} = \begin{cases} P_{BIC}^{*} & u_{dc} > u_{dc,Hmax} \\ P_{BIC}^{*}\dfrac{u_{dc} - u_{dc,Hmin}}{u_{dc,Hmax} - u_{dc,Hmin}} & u_{dc,Hmin} \le u_{dc} \le u_{dc,Hmax} \\ 0 & u_{dc,Lmin} \le u_{dc} \le u_{dc,Hmin} \\ -P_{BIC}^{*}\dfrac{u_{dc} - u_{dc,Lmin}}{u_{dc,Lmax} - u_{dc,Lmin}} & u_{dc,Lmax} \le u_{dc} \le u_{dc,Lmin} \\ -P_{BIC}^{*} & u_{dc} < u_{dc,Lmax}, \end{cases} \tag{2}$$

where, P_{BIC} is the active power transmitted by BIC, and P_{BIC}^{*} is the rating of the active power transmitted by BIC. $u_{dc,Hmin}$ is the minimum value of the upper limit set by the threshold of BIC, and $u_{dc,Hmax}$ is the maximum value set by the upper limit set by the threshold of BIC. $u_{dc,Lmin}$ is the minimum value set by the lower threshold, and $u_{dc,Lmax}$ is the maximum value set by the lower threshold. The improved droop control can be divided into three modes, as shown below:

(1) Inverter mode. When $u_{dc,Hmin} \le u_{dc} \le u_{dc,Hmax}$, u_{dc} does not reach the upper limit set of threshold value, BIC is in inverter mode. The DC sub-microgrid transmits active power to AC sub-microgrid through BIC, and the DC bus voltage is maintained stable by BIC. When $u_{dc} > u_{dc,Hmax}$, u_{dc} exceeds the threshold set limit, BIC is still in the inverter model. The power transmitted from the BIC to the AC sub-microgrid reaches the maximum value. The excess power in the DC sub-microgrid is charged for the energy storage system under the condition of unsaturated energy storage system. The energy storage system and BIC jointly maintain the DC bus voltage stability.

(2) Standby mode. When $u_{dc,Lmin} \le u_{dc} \le u_{dc,Hmin}$, DC bus voltage fluctuates in a small range, and excess or loss energy is provided by charging and discharging of the energy storage system to avoid unnecessary switching loss. At this point, the BIC is in standby mode without active power transmission, and the bus voltage stability is provided by the energy storage system.

(3) Rectifier mode. When $u_{dc,Lmax} \le u_{dc} \le u_{dc,Lmin}$, u_{dc} does not exceed the lower limit set by the

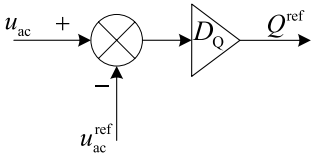

FIGURE 3. Reactive power control model.

threshold. The BIC is in the rectifier mode. The AC sub-microgrid transmits active power to the DC sub-microgrid through BIC, and the DC bus voltage is kept stable by the BIC. When $u_{dc} < u_{dc,Lmax}$, u_{dc} exceeds the lower limit set by the threshold, and the BIC is still in the rectifier mode. The power transmission from the AC sub-microgrid to the DC sub-microgrid reaches the maximum value. Under the condition of sufficient energy storage system, the BIC and the AC sub-microgrid maintain the DC bus voltage stability.

The improved BIC droop active power control increased the threshold setting and solved the switching loss caused by DC bus voltage fluctuation in a small range near the rated value. At the same time, it solves the difficulty and imprecision problem of traditional droop control due to the calculation of droop coefficient, and has the functions of bidirectional power flow and maintaining the voltage stability of DC bus.

The transmission of reactive power in the system, because the DC sub-microgrid does not exist reactive power problem. According to $Q - u_{ac}$droop control, reactive power flow of the BIC is only related to AC bus voltage amplitude [26]. The reactive power control of BIC is shown in Fig. 3.

Where, u_{ac} and u_{ac}^{ref} are the actual value and reference value of AC bus voltage, and the two are subtracted to obtain Δu_{ac}.Then, the reference value Q^{ref} of reactive power to be transmitted in the BIC is obtained by the droop control coefficient D_Q. In grid-connected mode, the voltage of AC bus is supported by the public grid. At the point, u_{ac} and u_{ac}^{ref} are equal, so $Q^{ref} = 0$. Therefore, in this article, the consumption of reactive power is all provided within the AC sub-microgrid, reducing its burden of power transmission [27].

C. CONTROL SYSTEM DESIGN

The design of the control system adopts double-loop control structure, and the outer loop is a power loop based on droop control, which controls the transmission of active power. The inner loop is the current loop, and the current tracing without static difference is realized by decoupling processing and PI controller. The control system design of BIC in AC/DC hybrid microgrid is shown in Fig. 4.

The respective meanings of each parameter in the figure are as follows: u_{dc} is the DC bus voltage; i_{dc} is the DC side current; C_{dc} is the filter capacitance on the DC side; $S_{a1} \sim S_{c2}$ is the power switch IGBT which is composed of a BIC; L, C is the filter inductance and filter capacitance that make up LC

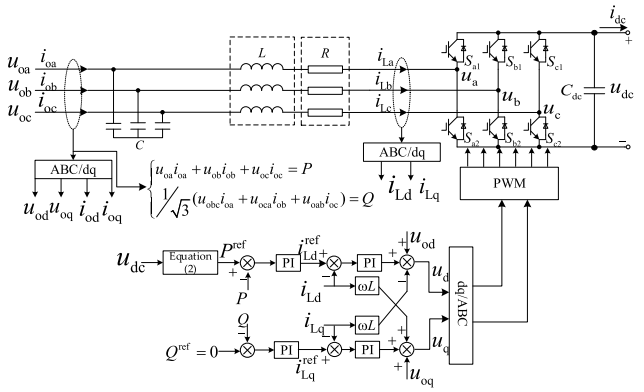

FIGURE 4. Design of BIC control system.

filter circuit. i_{Labc} is the inductance current on the AC side; u_{abc} is the three-phase voltage on the AC side of BIC; u_{oabc} is the three-phase voltage of AC bus; i_{oabc} is the output of three - phase current for ac bus.

The first is the power control part. The BIC detects the DC bus voltage and calculates the reference value P^{ref} of the BIC transmission power through equation (2). According to the power calculation equation (3), the instantaneous active power P and reactive power Q output by the bidirectional converter can be obtained.

$$\begin{cases} u_{oa}i_{oa} + u_{ob}i_{ob} + u_{oc}i_{oc} = P \\ 1/\sqrt{3}(u_{obc}i_{oa} + u_{oca}i_{ob} + u_{oab}i_{oc}) = Q. \end{cases} \tag{3}$$

By subtracting the actual value from the reference value of power transmission, the reference value i_{Ld}^*, i_{Lq}^* of inductance current of d axis and q axis is obtained by PI controller, and then it is controlled by inner current loop. The current inner loop control is as follows.

The switching function of BIC is defined as follows:

$$S_k = \begin{cases} 0 & \text{lower arm on, upper arm off} \\ 1 & \text{upper arm on, lower arm off} \end{cases}, k = a, b, c. \tag{4}$$

The three-phase voltage at AC side of BIC can be obtained as follows:

$$u_{abc} = S_k u_{dc}, \quad k = \text{a,b,c}. \tag{5}$$

According to Kirchhoff's law, the mathematical model of BIC in three-phase static coordinate system is established, as shown in equation (6).

$$\begin{cases} L\dfrac{di_{Labc}}{dt} + Ri_{Labc} = u_{oabc} - u_{abc} - u_{NO} \\ C\dfrac{du_{dc}}{dt} = i_a S_a + i_b S_b + i_c S_c - i_{dc}, \end{cases} \tag{6}$$

where, u_{NO} is the neutral point voltage at the AC side of BIC. In the ideal working condition, the three-phase symmetry of

AC bus voltage and the zero sequence component of current is 0. The equation (7) can be obtained as follows:

$$u_{\mathrm{NO}} = -\frac{u_{\mathrm{dc}}}{3}(S_{\mathrm{a}} + S_{\mathrm{b}} + S_{\mathrm{c}}). \tag{7}$$

The physical meaning of the mathematical model of BIC in three phase static coordinate system is clear and intuitive. However, AC side voltage and current are time-varying variables in the system, which is not conducive to the analysis and design of the controller. Therefore, to convert the three-phase sine component into the DC component, the three-phase static coordinate system can be converted into a two-phase synchronous rotation d-q coordinate system by means of three-dimensional transformation [28], as follows:

$$\begin{cases} L\dfrac{di_{\mathrm{Ld}}}{dt} + Ri_{\mathrm{Ld}} = u_{\mathrm{od}} - u_{\mathrm{d}} + \omega Li_{\mathrm{Lq}} \\ L\dfrac{di_{\mathrm{Lq}}}{dt} + Ri_{\mathrm{Lq}} = u_{\mathrm{oq}} - u_{\mathrm{q}} - \omega Li_{\mathrm{Ld}} \\ C\dfrac{du_{\mathrm{dc}}}{dt} = \dfrac{3}{2}(i_{\mathrm{Ld}}S_{\mathrm{d}} + i_{\mathrm{Lq}}S_{\mathrm{q}}) - i_{\mathrm{dc}}. \end{cases} \tag{8}$$

From equation (8), it can be seen that under the d-q coordinate system with two-phase synchronous rotation, the d-axis and q-axis components have coupling components and need decoupling control [29]. The decoupling equation (9) is shown below.

$$\begin{cases} u_{\mathrm{d}} = -(k_{\mathrm{ip}} + \dfrac{k_{\mathrm{ii}}}{s})(i^*_{\mathrm{Ld}} - i_{\mathrm{Ld}}) + u_{\mathrm{od}} - \omega Li_{\mathrm{Lq}} \\ u_{\mathrm{q}} = -(k_{\mathrm{ip}} + \dfrac{k_{\mathrm{ii}}}{s})(i^*_{\mathrm{Lq}} - i_{\mathrm{Lq}}) + u_{\mathrm{oq}} + \omega Li_{\mathrm{Ld}}, \end{cases} \tag{9}$$

where k_{ip}, k_{ii} are the proportional and integral coefficients of the current loop PI controller respectively, and i^*_{Ld}, i^*_{Lq} are the reference currents of the inductance of d-axis and q-axis respectively.

III. HARMONIC DETECTION METHOD

A. FBD HARMONIC CURRENT DETECTION METHOD

The traditional FBD harmonic current detection method was first proposed by Fryzc and improved by Buchholz and Depenbrock. The basic idea of FBD is to convert the load in the actual circuit into an ideal conductance element. In this method, the power consumption in the circuit can be equivalent to the conductivity consumption without other energy loss. According to the decomposition characteristic of equivalent conductance to the current, the compensated current component can be calculated to suppress the system harmonic current [7].

According to literature [30], the current in the three-phase three-wire system can be divided into positive sequence component and negative sequence component, and the three-phase current to be treated is shown in equation (10).

$$\begin{cases} i_{\mathrm{a}} = \sum\limits_{n=1}^{\infty}[i_n^+ \sin(n\omega t + \varphi_n^+) + i_n^- \sin(n\omega t + \varphi_n^-)] \\ i_{\mathrm{b}} = \sum\limits_{n=1}^{\infty}[i_n^+ \sin(n\omega t + \varphi_n^+ - 120^\circ) \\ \quad + i_n^- \sin(n\omega t + \varphi_n^- + 120^\circ)] \\ i_{\mathrm{c}} = \sum\limits_{n=1}^{\infty}[i_n^+ \sin(n\omega t + \varphi_n^+ + 120^\circ) \\ \quad + i_n^- \sin(n\omega t + \varphi_n^- - 120^\circ)], \end{cases} \tag{10}$$

where, i_n^+ is the amplitude of the positive sequence component of current, i_n^- is the amplitude of the negative sequence component of current, φ_n^+ is the initial phase angle of the positive sequence component, and φ_n^- is the initial phase angle of the negative sequence component.

The traditional FBD harmonic detection method uses PLL to generate the reference voltage which is in phase with three-phase grid voltage, instead of the actual value. The three-phase reference voltage is:

$$\begin{cases} u_{\mathrm{a}} = \sin(\omega t) \\ u_{\mathrm{b}} = \sin(\omega t - 120^\circ) \\ u_{\mathrm{c}} = \sin(\omega t + 120^\circ). \end{cases} \tag{11}$$

According to equation (12), the equivalent active conductance is calculated as follows:

$$\begin{aligned} G_P(t) &= \frac{u_{\mathrm{a}}i_{\mathrm{a}} + u_{\mathrm{b}}i_{\mathrm{b}} + u_{\mathrm{c}}i_{\mathrm{c}}}{u_{\mathrm{a}}^2 + u_{\mathrm{b}}^2 + u_{\mathrm{c}}^2} \\ &= \sum_{n=1}^{\infty} i_n^+ \cos[(n-1)\omega t + \varphi_n^+] \\ &\quad - \sum_{n=1}^{\infty} i_n^- \cos[(n+1)\omega t + \varphi_n^-]. \end{aligned} \tag{12}$$

The calculate of equivalent reactive conductance requires 90° phase shift of three-phase voltage phase as follows:

$$\begin{cases} u^*_{\mathrm{a}} = \cos(\omega t) \\ u^*_{\mathrm{b}} = \cos(\omega t - 120^\circ) \\ u^*_{\mathrm{c}} = \cos(\omega t + 120^\circ). \end{cases} \tag{13}$$

Then the equivalent reactive conductivity can be obtained as follows:

$$\begin{aligned} G_Q(t) &= \frac{u^*_{\mathrm{a}}i_{\mathrm{a}} + u^*_{\mathrm{b}}i_{\mathrm{b}} + u^*_{\mathrm{c}}i_{\mathrm{c}}}{u_a^{*2} + u_b^{*2} + u_c^{*2}} \\ &= \sum_{n=1}^{\infty} i_n^+ \sin[(n-1)\omega t + \varphi_n^+] \\ &\quad - \sum_{n=1}^{\infty} i_n^- \sin[(n+1)\omega t + \varphi_n^-]. \end{aligned} \tag{14}$$

The equivalent active and reactive conductance are filtered through LPF to remove the AC component in the conductance while retaining the DC component. The filtered conductance

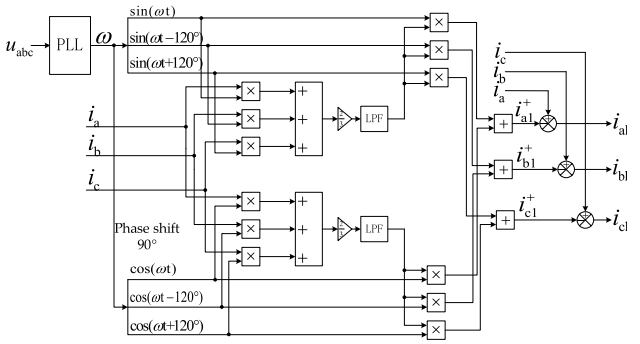

FIGURE 5. Traditional FBD harmonic current detection method.

value is the equivalent conductance of the fundamental wave, as follows:

$$\begin{cases} G_{Pf}(t) = i_1^+ \cos\varphi_1^+ \\ G_{Qf}(t) = i_1^+ \sin\varphi_1^+, \end{cases} \tag{15}$$

The active and reactive conductance are multiplied by the corresponding reference voltage to obtain the active and reactive current components of the three-phase fundamental wave. The three-phase fundamental positive sequence current component is obtained by adding the conductance current components of corresponding phase:

$$\begin{cases} i_{a1}^+ = G_{Pf}(t)\cdot u_a + G_{Qf}(t)\cdot u_a^* \\ \quad = i_1^+(\sin(\omega t)\cos\varphi_1^+ + \cos(\omega t)\sin\varphi_1^+) \\ \quad = i_1^+\sin(\omega t+\varphi_1^+) \\ i_{b1}^+ = G_{Pf}(t)\cdot u_b + G_{Qf}(t)\cdot u_b^* = i_1^+\sin(\omega t+\varphi_1^+-120^\circ) \\ i_{c1}^+ = G_{Pf}(t)\cdot u_b + G_{Qf}(t)\cdot u_b^* = i_1^+\sin(\omega t+\varphi_1^+ +120^\circ). \end{cases} \tag{16}$$

Finally, the harmonic current component of each phase can be obtained by subtracting the fundamental current component from the original current. The harmonic current component obtained is:

$$i_{abc,h} = i_{abc} - i_{abc1}^+. \tag{17}$$

In summary, FBD harmonic current detection method does not require complex matrix transformation and is not affected by the zero-sequence current component. It can directly detect the positive sequence active and reactive current components of the fundamental wave current. The principle of FBD harmonic current detection method is shown in Fig. 5.

However, the effect of traditional PLL is not ideal, which affects the output of system frequency signal. In the system, the cutoff frequency of LPF can not consider the response speed and tracking speed of FBD algorithm. Therefore, FBD algorithm needs to be improved.

B. DDSRF-PLL

The DDSRF-PLL has a self-decoupling network, which can eliminate the negative sequence fundamental frequency component [31]. Therefore, accurate phase detection can also be

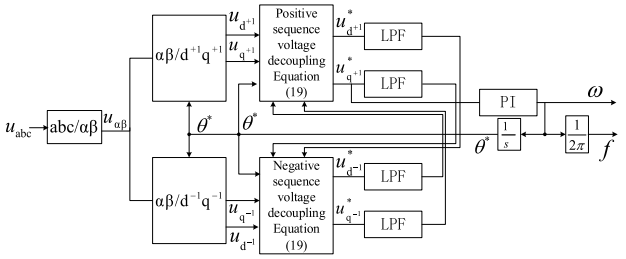

FIGURE 6. DDSRF-PLL structure schematic diagram.

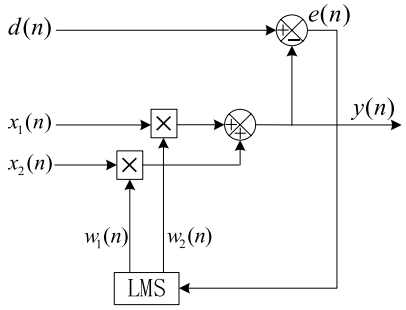

FIGURE 7. Adaptive filter based on LMS algorithm.

realized when the grid-connected state is affected by nonlinear load. According to literature [32], the three-phase voltage u_{abc} is transformed to the two-phase static coordinate system $u_{\alpha\beta}$ by Clarke, which can offset the zero-sequence component and eliminate the influence of zero-sequence component. When u_α and u_β are sent into Park transform module $T_{dq^{+1}}$ and $T_{dq^{-1}}$, the positive and negative sequence voltage components are obtained as follows:

$$\begin{cases} \begin{bmatrix} u_{d^{+1}} \\ u_{q^{+1}} \end{bmatrix} = \begin{bmatrix} \cos(\omega^* t) & \sin(\omega^* t) \\ -\sin(\omega^* t) & \cos(\omega^* t) \end{bmatrix} \begin{bmatrix} u_\alpha \\ u_\beta \end{bmatrix} \\ \begin{bmatrix} u_{d^{-1}} \\ u_{q^{-1}} \end{bmatrix} = \begin{bmatrix} \cos(\omega^* t) & -\sin(\omega^* t) \\ \sin(\omega^* t) & \cos(\omega^* t) \end{bmatrix} \begin{bmatrix} u_\alpha \\ u_\beta \end{bmatrix}. \end{cases} \tag{18}$$

In order to suppress the oscillation in the coordinate system d^{+1} and q^{+1}, d^{+1} and q^{+1} should be switched into the self-decoupling network, and the positive and negative sequence voltage after decoupling is obtained as follows:

$$\begin{cases} \begin{bmatrix} u_{d^{+1}}^* \\ u_{q^{+1}}^* \end{bmatrix} = \begin{bmatrix} u_{d^{+1}} - [u_{d^{-1}}^* \cdot \cos(2\theta^*) - u_{q^{-1}}^* \cdot \sin(2\theta^*)] \\ u_{q^{+1}} - [u_{d^{-1}}^* \cdot \sin(2\theta^*) + u_{q^{-1}}^* \cdot \cos(2\theta^*)] \end{bmatrix} \\ \begin{bmatrix} u_{d^{-1}}^* \\ u_{q^{-1}}^* \end{bmatrix} = \begin{bmatrix} u_{d^{-1}} - [u_{d^{+1}}^* \cdot \cos(2\theta^*) + u_{q^{+1}}^* \cdot \sin(2\theta^*)] \\ u_{q^{-1}} - [-u_{d^{+1}}^* \cdot \sin(2\theta^*) + u_{q^{+1}}^* \cdot \cos(2\theta^*)] \end{bmatrix}. \end{cases} \tag{19}$$

Finally, the PI controller is used to make $u_{q^{+1}}^* = 0$ to keep synchronization and realize phase-locked, thus obtaining the frequency and phase information of three-phase voltage. The structural principle of DDSRF-PLL is shown in Fig. 6.

C. ADAPTIVE FILTER BASED ON LMS

Adaptive filter is composed of digital filter with adjustable parameters and adaptive algorithm. It can continuously adjust

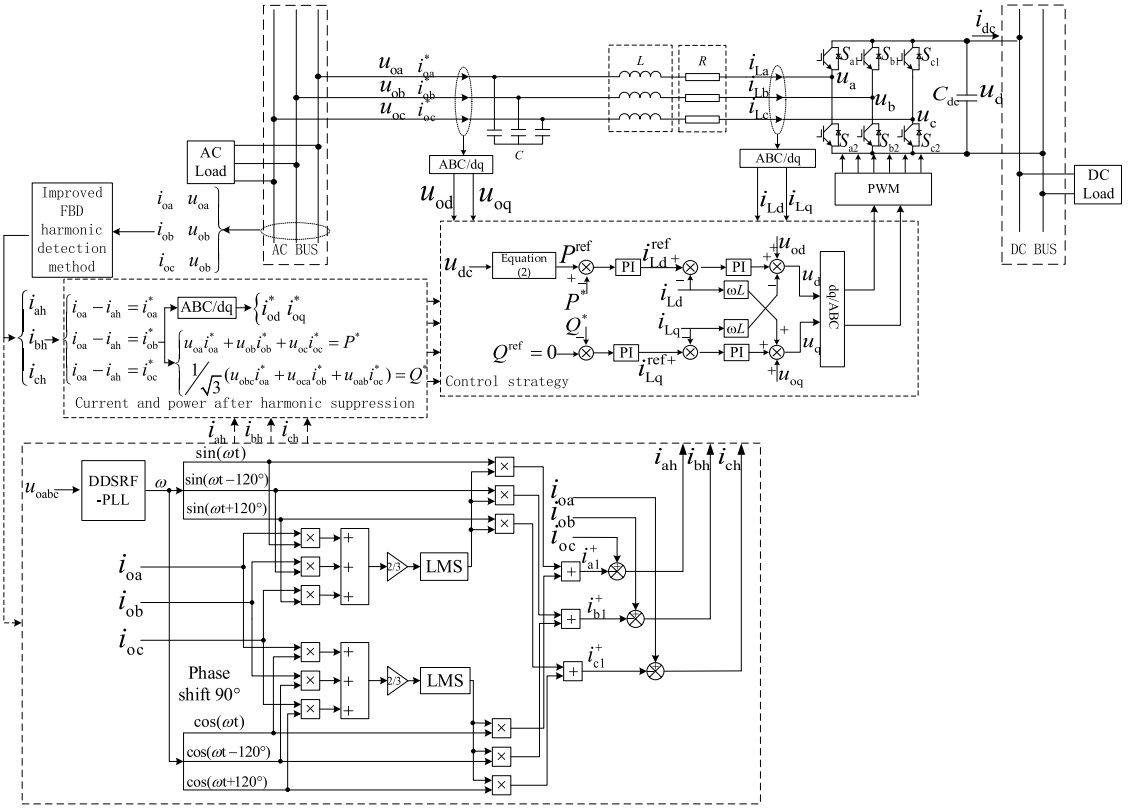

FIGURE 8. Improved harmonic suppression control strategy for BIC.

filter parameters through adaptive algorithm according to the change of input characteristics, so as to realize accurate tracking of reference signals [33].

At present, the commonly used adaptive algorithms include least mean square (LMS) algorithm and recursive least power (RLS) algorithm. RLS algorithm has fast convergence speed but large amount of computation. Compared with RLS algorithm, LMS algorithm requires less computation, does not need complex matrix transformation, and is easy to implement. So the research of adaptive filter is mainly in LMS algorithm. The principle of adaptive filter based on LMS algorithm is shown in Fig. 7.

According to Fig. 7, the signal to be measured $d(n)$ subtracts the filter output signal $y(n)$ to form an error signal $e(n)$. $x_1(n)$ and $x_2(n)$ are power grid phase locked sine and cosine signals. The weight coefficient $w_1(n)$ and $w_2(n)$ of error signal $e(n)$ are obtained by LMS algorithm, and the weights of $x_1(n)$ and $x_2(n)$ are adjusted dynamically. The output signal $y(n)$ of the filter approximates the fundamental current signal, and then $e(n)$ can be approximately equal to the harmonic current signal. The adaptive harmonic detection method based on LMS algorithm can be realized by equation (20).

$$\begin{cases} y(n) = x_1(n) \cdot w_1(n) + x_2(n) \cdot w_2(n) \\ e(n) = d(n) - y(n) \\ w_1(n+1) = w_1(n) + 2\mu e(n) \cdot x_1(n) \\ w_2(n+1) = w_2(n) + 2\mu e(n) \cdot x_2(n), \end{cases} \tag{20}$$

where, μ is the step length, $x_1(n)$ and $x_2(n)$ are the sines and cosines after the phase-locked voltage of the power grid. $d(n)$ is composed of fundamental current signal and harmonic current signal, considering that it is combined with FBD harmonic current detection method. The filtering process of active conductance $G_P(t)$ is similar to that of reactive conductance $G_Q(t)$. Take the filtering process of $G_P(t)$ as an example, where $d(n) = G_P(t)$. $x_1(n)$ and $x_2(n)$ can be replaced by the sines and cosines generated by DDSRF-PLL phase locking signals $u_{\text{DDSRF-PLL}}$ and $u^*_{\text{DDSRF-PLL}}$. Then equation (20) can be adjusted as:

$$\begin{cases} y(n) = u_{\text{DDSRF-PLL}} \cdot w_1(n) + u^*_{\text{DDSRF-PLL}} \cdot w_2(n) \\ e(n) = G_P(t) - y(n) \\ w_1(n+1) = w_1(n) + 2\mu e(n) \cdot u_{\text{DDSRF-PLL}} \\ w_2(n+1) = w_2(n) + 2\mu e(n) \cdot u^*_{\text{DDSRF-PLL}}. \end{cases} \tag{21}$$

IV. ANALYSIS OF SIMULATION RESULTS

A. DROOP CONTROL STRATEGY BASED ON IMPROVED FBD METHOD

In grid-connected mode, when the system operates under ideal conditions, the droop control strategy can not only realize the BIC power flow between the two sub-microgrids, but also maintain the stability of the DC bus voltage together with the energy storage system. When there are nonlinear loads in the system, the output current of AC bus will be distorted and the output power will be greatly disturbed, which will

TABLE 1. Related parameters of AC/DC hybrid microgrid.

Symbol	Parameters	Value
u_{ac}^{ref}	AC bus rated line voltage	380V
f^{ref}	AC bus rated frequency	50Hz
u_{dc}^{ref}	DC bus rated frequency	700V
P_{ac}^{max}	AC sub-microgrid capacity	30kW
P_{dc}^{max}	DC sub-microgrid capacity	20kW
S	BIC capacity	20kVA
P_{ac_load}	Initial AC load	14kW
P_{dc_load}	Initial DC load	12kW

affect the stability and security of the whole microgrid system. In order to suppress the harmonic current in the circuit in the presence of nonlinear load. Firstly, FBD harmonic current detection method is needed to detect the harmonic current component in nonlinear load. The traditional FBD harmonic current detection method also has some problems. When the grid voltage and current are distorted, the traditional PLL is not ideal. The improved FBD harmonic detection method uses DDSRF-PLL instead of the traditional PLL to eliminate the influence of the negative sequence component on the positive sequence component. The cutoff frequency of the LPF cannot give consideration to the response speed and detection accuracy of the FBD method at the same time. The adaptive filter based on the LMS algorithm is adopted to automatically adjust the parameters so that the algorithm can accurately and quickly detect the fundamental wave current component.

Then, on the basis of droop control strategy, combined with FBD harmonic current detection method, the harmonic current in nonlinear load is extracted. The harmonic current is suppressed by modifying the current at the output of AC bus. Minimizes the fluctuation of the output power of the AC bus to the BIC. Combined with analysis, a control strategy based on improved harmonic suppression droop control is designed, as shown in Fig. 8. The simulation model was built by Maltlab/ Simulink software, and the simulation results of the improved harmonic suppression control strategy proposed in this article and the traditional FBD harmonic suppression control strategy in literature [20] were compared under ideal working conditions and nonlinear load respectively.

In this article, the battery energy storage system is designed as an ideal condition, and the situation of oversaturation and insufficient power is not considered temporarily. Relevant parameters in the simulation system are shown in Table 1, where the power is active power.

In grid-connected operation, there is no linear load in the AC/DC hybrid microgrid, and the AC bus is directly connected to the public grid, so there is no need to analyze the frequency and voltage changes of the AC side sub-microgrid. The DC bus voltage rating is 700V. For stable operation of the system, the DC bus voltage fluctuation should not exceed

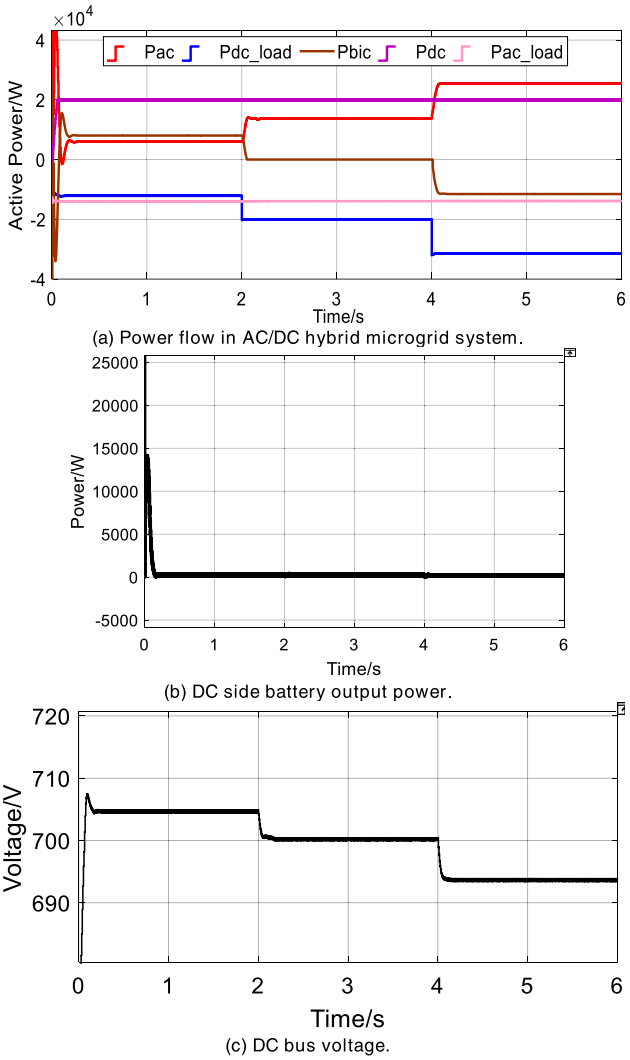

FIGURE 9. System simulation results under ideal operating conditions.

10%. Therefore, set the threshold value. The upper maximum value is 711V and the upper minimum value is 701V. The lower limit maximum value is 689V and the minimum value is 699V. The DC sub-microgrid capacity is 20kW, the AC sub-microgrid capacity is 30kW, and the rated capacity of the BIC is 20kVA. The initial load in the AC sub-microgrid is 14kW, and the initial load in the DC sub-microgrid is 12kW. The load characteristics are all resistive load. At different times, the load is increased so that the BIC can make the judgment of power flow direction and realize the bidirectional flow of power between AC-DC sub-microgrid.

B. IDEAL WORKING CONDITION

The system works in the ideal condition, without considering the energy consumed by the transmission line. The simulation results of the control strategy are shown in Fig. 9.

P_{ac} is the generating power of AC sub-microgrid, P_{ac_load} is the load of AC sub-microgrid, P_t is the active power transmitted by BIC, P_{dc} is the generating power of DC subnet, and

P_{dc_load} is the load power of DC. The initial time of 0-0.2s is the start-up stage. As can be seen from Fig. 9(a) that the DC side grid starts to generate electricity from the generation unit and gradually climbs from 0 to the maximum power point. At this time, it can be seen from Fig. 9(c) that the DC bus voltage $u_{dc} < u_{dc,Lmax}$, it is less than the maximum value of the lower limit of threshold, the battery energy storage system and the BIC jointly maintain the DC bus voltage stability. It can be seen from Fig. 9(b) that the battery energy storage system gradually supplies power to the DC sub-microgrid when the DC bus voltage is lower than 689V, and when the DC bus voltage is higher than 699V, the power supply gradually drops to 0.

0.2s-2s in inverter mode. At 0.2s, the power generation unit in the DC sub-microgrid reaches the maximum power point, generating capacity is 20kW, DC side load is 12kW, and DC bus voltage is 705V. At this time $u_{dc,Hmin} < u_{dc} < u_{dc,Hmax}$. u_{dc} is between the maximum and minimum value of the upper limit of threshold setting, and the energy storage system is in standby state. The energy supply exceeds demand in the DC sub-microgrid, and the excess energy flows to the AC sub-microgrid through the BIC. The BIC is in inverter mode and transmits 8kW power to the AC sub-microgrid. The AC sub-microgrid load is shared by the AC sub-microgrid and DC sub-microgrid, so the AC sub-microgrid only needs 6kW of power generation to achieve the power balance within the whole system.

2s-4s in standby mode. At 2s, the DC sub-microgrid increases 8kW load, and the total DC load is 20kW. The energy in the DC sub-microgrid is balanced. The DC bus voltage is 700V, at $u_{dc,Lmin} < u_{dc} < u_{dc,Hmin}$, there is no extra power. The BIC is in standby state, the AC load is assumed by the AC sub-microgrid, and the AC sub-microgrid generates 14kW power to achieve the energy balance within the whole system.

4s-6s in rectifier mode. At 4s, the DC sub-microgrid continues to increase the load of 12kW, the DC total load increases to 32kW, and the DC bus voltage drops to 693V. At this time, $u_{dc,Lmax} < u_{dc} < u_{dc,Lmin}$, u_{dc} is between the maximum and minimum value of the lower limit set by the threshold, and the energy in the DC sub-microgrid is in short supply. The BIC is in the rectifier mode. The AC sub-microgrid transmits 12kW to the DC sub-microgrid, and the DC load is jointly assumed by the AC sub-microgrid and DC sub-microgrid. The AC sub-microgrid generates 26kW power, 14kW is used for AC load consumption, and 12kW is transmitted to the DC sub-microgrid through BIC to achieve power balance in the whole system. It is verified that the designed control strategy can control the BIC to maintain the stability of DC bus voltage and power bidirectional flow.

The voltage and current of ac sub-microgrid are shown in Fig. 10.

As can be seen from Fig. 10, the voltage within the AC sub-microgrid is stable at 311V because the support of the utility network does not change with the transmitted power. The current will change with the amount of transmitted power.

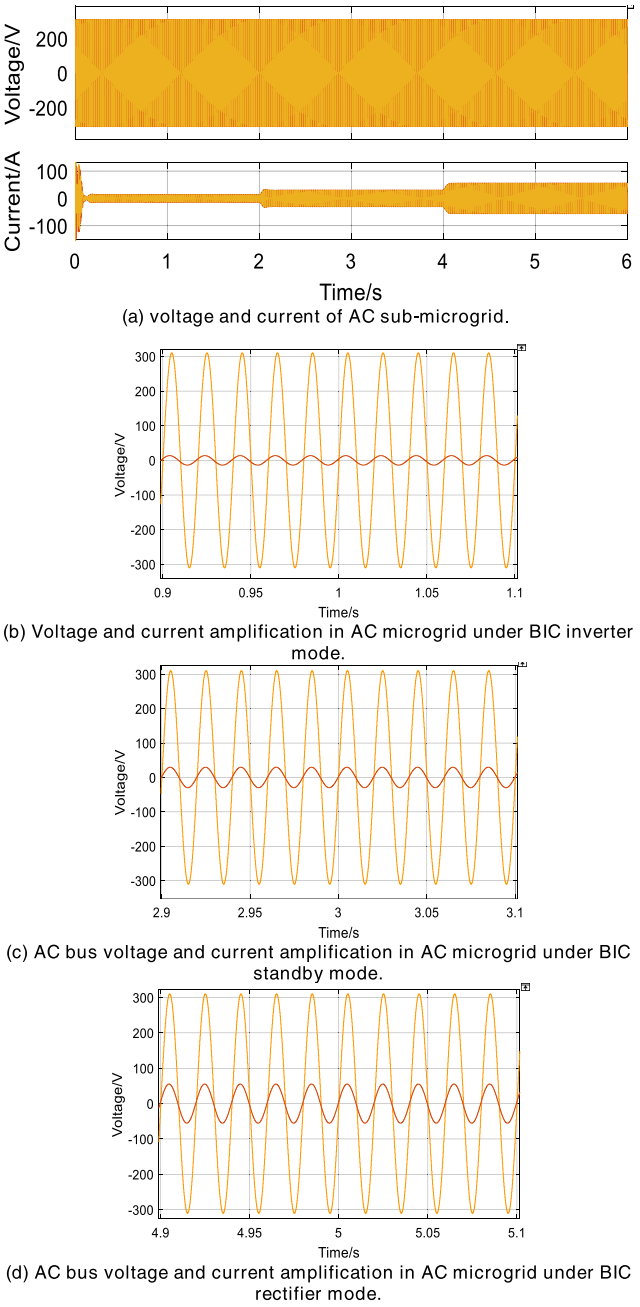

FIGURE 10. Voltage and current of AC sub-microgrid under ideal conditions.

After 0.2s, the current of AC sub-microgrid keeps increasing. Compared with the power curve of AC/DC sub-microgrid in Fig. 9(a), it increases with the increase of output power. A-phase voltage and current on AC side of BIC are shown in Fig. 11.

In Fig. 11, 0.65s-0.9s and 4.65s-4.9s were amplified respectively. The system is set to flow from the DC side to the AC side as the positive reference direction. It can be seen from Fig. 11 that the A-phase voltage and current on the AC side are in the same phase, and the power flows from the DC side to the AC side, so the BIC is in the inverter mode. 2s-4s,

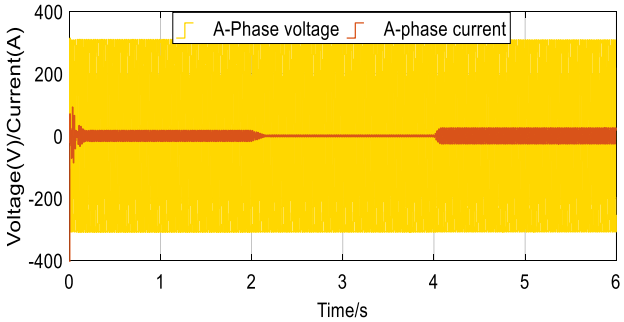

(a) A-phase voltage and current on AC side of BIC.

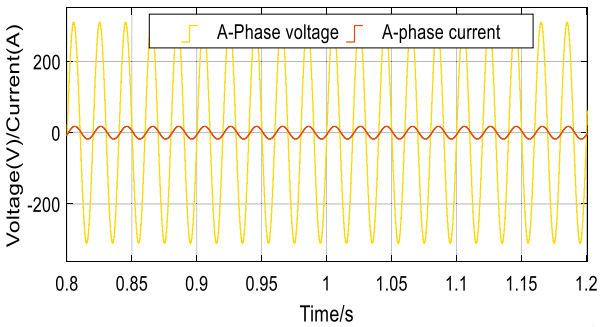

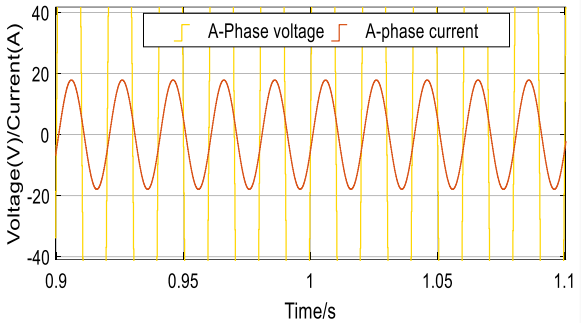

(b) A-phase voltage and current on amplification in BIC inverter mode.

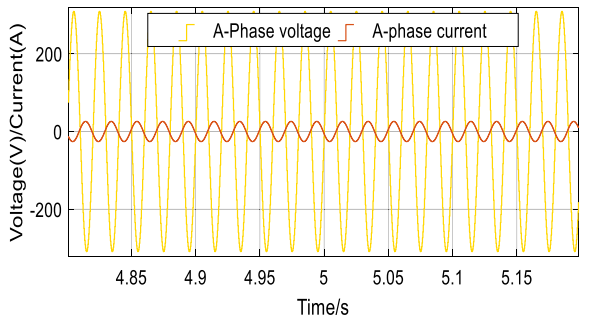

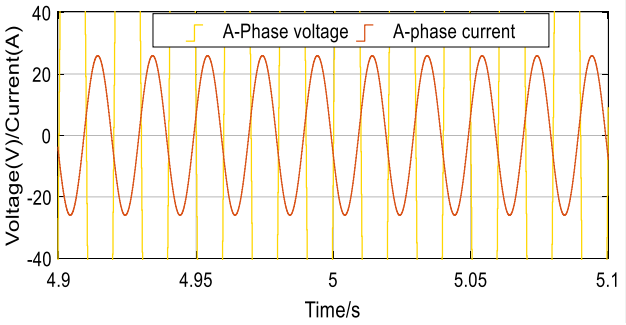

(c) A-phase voltage and current on amplification in BIC rectifier mode.

FIGURE 11. **A-phase voltage and current on AC side of BIC under ideal conditions.**

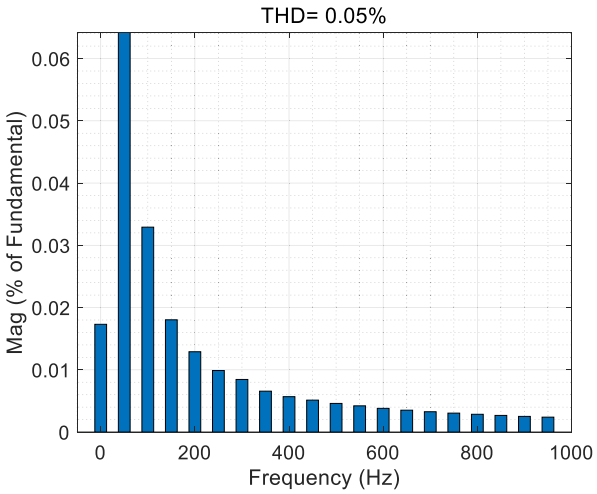

(a) THD of AC side output current in BIC inverter mode.

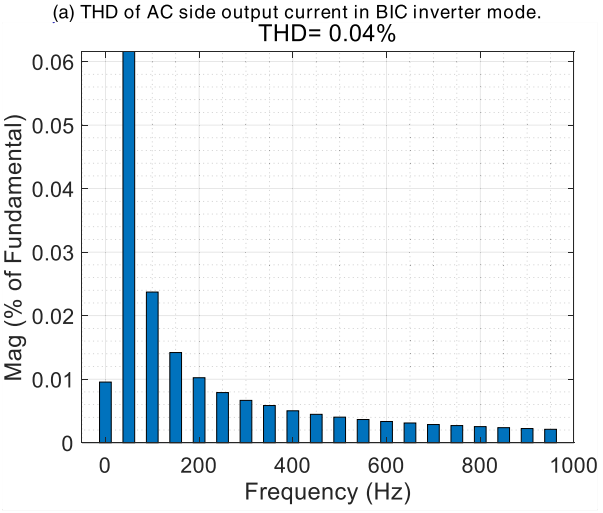

(b) THD of AC side output current in BIC rectifier mode.

FIGURE 12. **THD of BIC output current under ideal condition.**

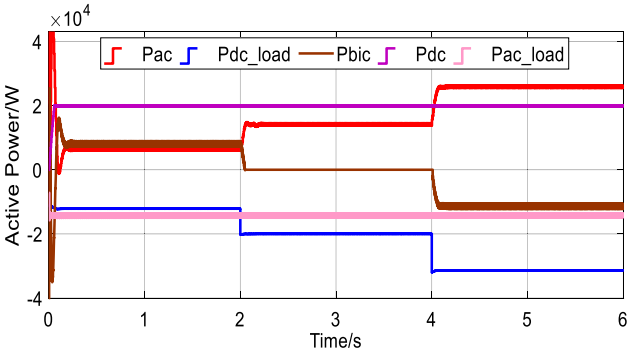

FIGURE 13. **Only droop control strategy simulation results under nonlinear load conditions.**

A-phase current is basically 0, BIC is in standby state. 4s-6s, AC side A-phase voltage and current reverse phase, power from the AC side to the DC side, and the BIC in the rectifier mode. The BIC in Fig. 11 is consistent with the results in Fig. 9.

Under ideal working conditions, there is no nonlinear load in the system. The THD output by the AC side of the BIC is shown in Fig. 12.

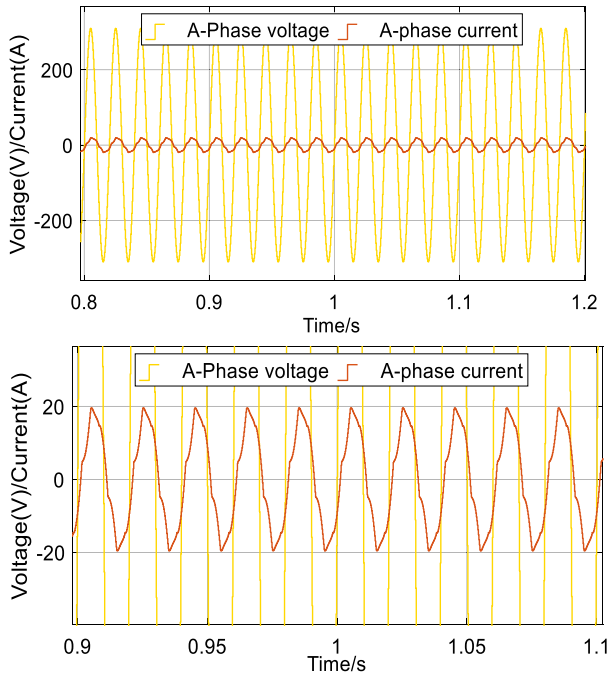

(a) A-phase voltage and current on amplification in BIC inverter mode.

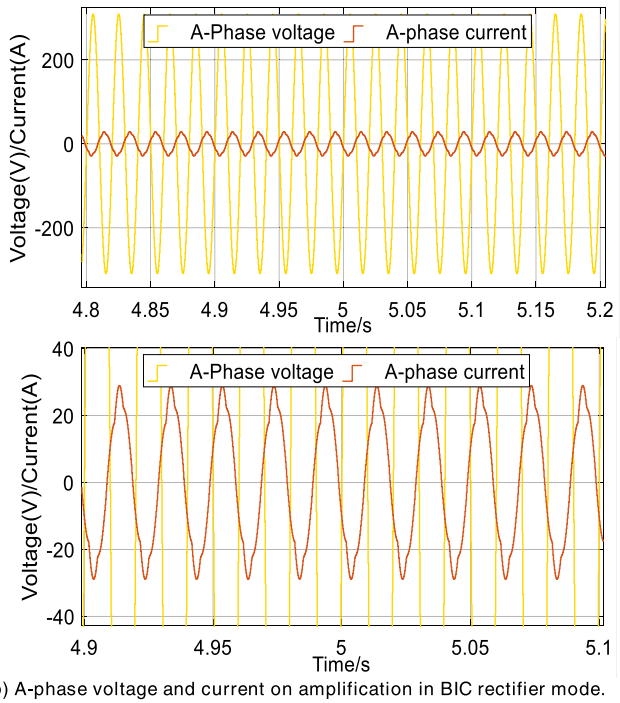

(b) A-phase voltage and current on amplification in BIC rectifier mode.

FIGURE 14. Only droop control BIC AC side A-phase voltage and current under nonlinear load.

Figure 12 shows the degree of THD of the AC side output of the BIC in inverter mode and rectifier mode respectively after the system operates statically. In 0.2s-2s inverter mode, THD is 0.05%. The THD is 0.04% in 4s-6s rectifier mode. The THD is less than 1% both inverter mode and rectifier mode, which meets the power quality standards.

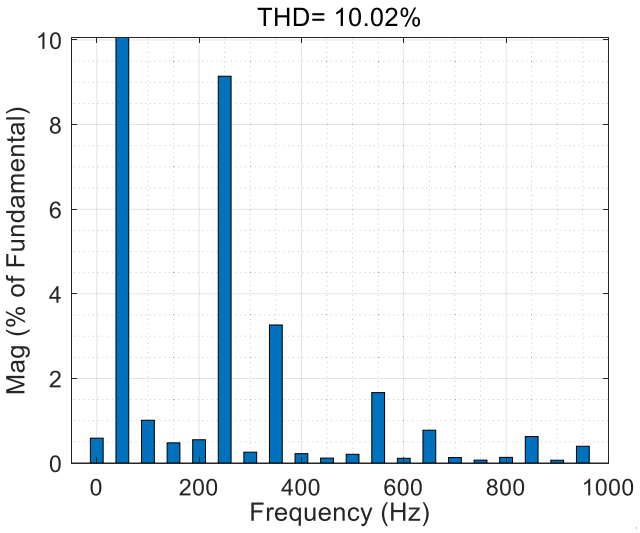

(a) THD of AC side output current in BIC inverter mode.

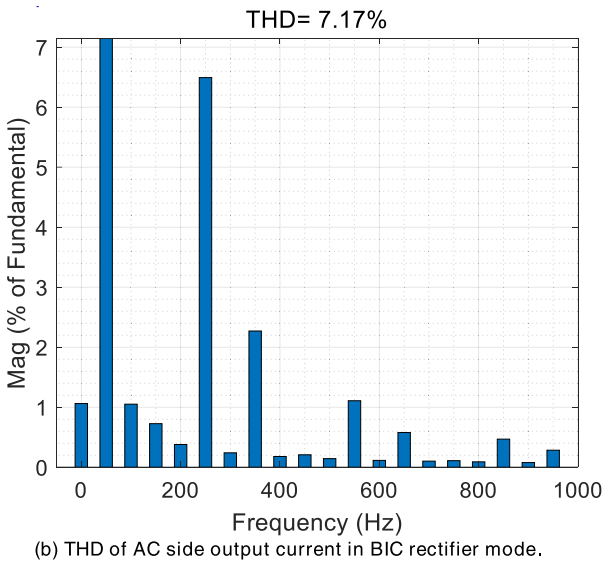

(b) THD of AC side output current in BIC rectifier mode.

FIGURE 15. Only droop control BIC AC side A-phase current THD.

C. NON-IDEAL WORKING CONDITION

When the nonlinear load is added into the system, the waveform is similar to the ideal condition. The AC bus current will be distorted and generate harmonic current, which will disturb the transmission power in BIC and affect the stability of the system. Under the nonlinear load condition, the simulation results of only droop control strategy are shown in Fig. 13.

In the ideal working condition, the AC side load is 14kW linear load. In order to verify the feasibility and effectiveness of the design method, the AC load is composed of 7kW linear load and 7kW nonlinear load under non-ideal conditions. By comparing Fig. 13 with Fig. 9(a), the BIC can realize the power flow between two sub-microgrids and maintain the balance between the whole system. However, the AC load consumption power and BIC transmission power will be significantly disturbed. After adding non-linear load, only

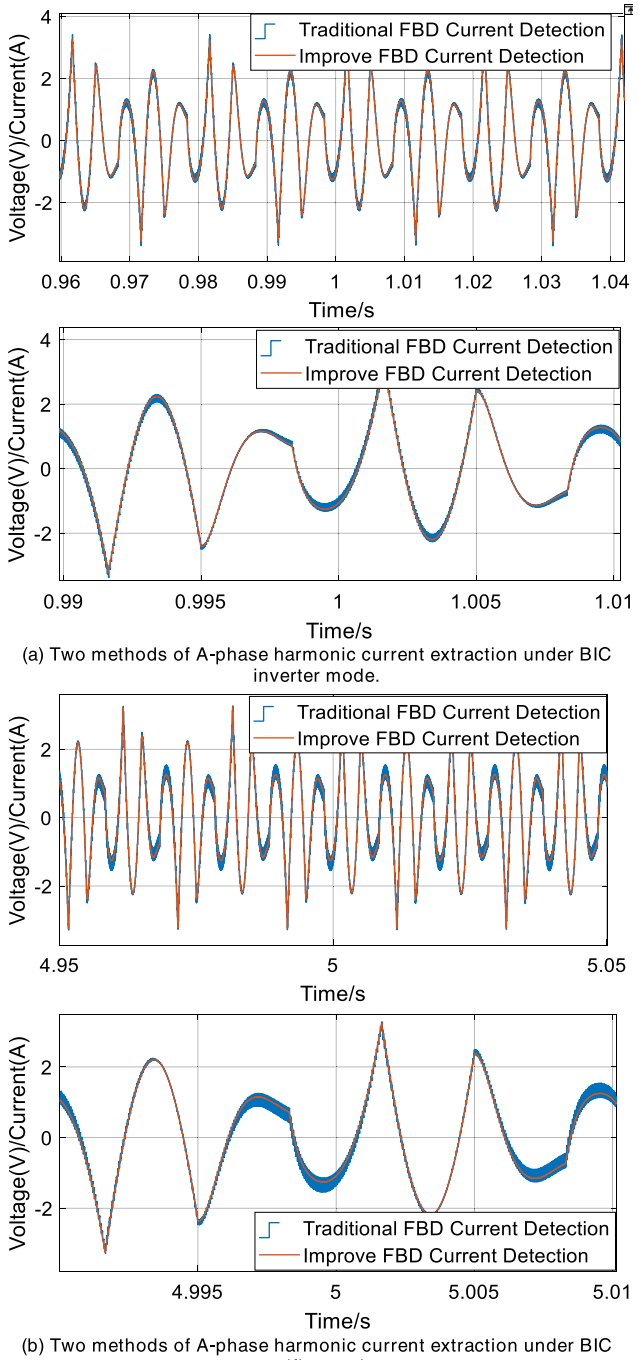

(a) Two methods of A-phase harmonic current extraction under BIC inverter mode.

(b) Two methods of A-phase harmonic current extraction under BIC rectifier mode.

FIGURE 16. Two methods for A-phase harmonic current extraction under nonlinear load.

droop control strategy is used for the AC side A-phase current of the BIC as shown on Fig.14.

In order to facilitate observation, both inverter and rectifier parts are amplified. Because the current is very small in the standby mode of 2s∼4s, no observation is made. As can be seen from Fig. 14, the A-phase current sinusoidal curve on the AC side of the BIC is obviously distorted. And the THD can be obtained through Fourier transform analysis, as shown in Fig. 15.

TABLE 2. Main harmonic content.

Number	Inverter mode harmonic content (%)	Rectifier mode harmonic content (%)
5	9.19%	6.53%
7	3.24%	2.21%
11	1.76%	1.18%
13	0.78%	0.57%
17	0.69%	0.42%
19	0.40%	0.36%

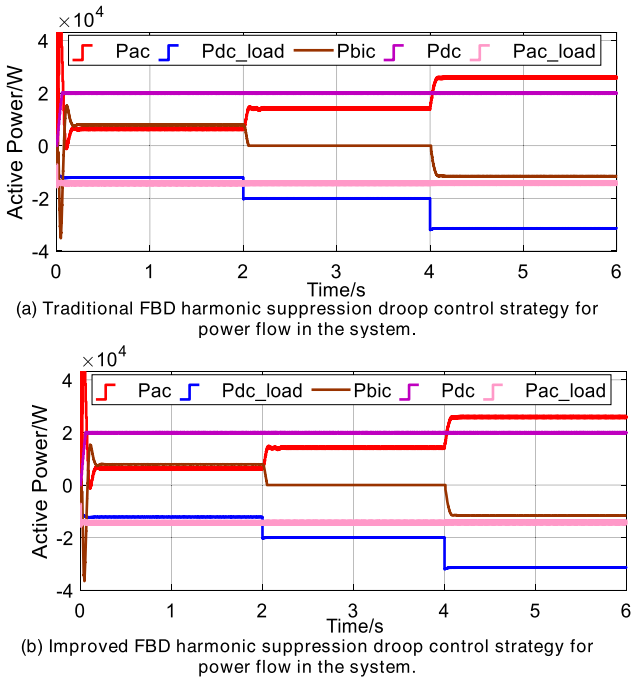

(a) Traditional FBD harmonic suppression droop control strategy for power flow in the system.

(b) Improved FBD harmonic suppression droop control strategy for power flow in the system.

FIGURE 17. Power transmission of harmonic suppression droop control strategy.

It can be seen from Fig. 15 that the main harmonics are the 5th, 7th and 11th harmonics, and the harmonic content is shown in Table 2. The total harmonic distortion of BIC in inverter mode and rectifying mode is 10.02% and 7.17% respectively, which is greater than the allowable limit of 5% in IEEE standard. Therefore, the power quality transmitted in BIC is unqualified, needs to be treated.

The traditional FBD harmonic current detection method and the improved FBD harmonic current detection method are respectively used to extract the A-phase current on the AC side of the BIC, as shown in Fig. 16.

For the convenience of observation, the inverter part and the rectifier part were amplified. Because the current is very small in 2s∼4s standby mode, no observation is made. It can be seen from Fig. 16 that the improved FBD can effectively suppress the oscillation in the current and achieve more accurate tracking of the harmonic current.

The traditional FBD suppression harmonic droop control strategy and the improved FBD suppression harmonic droop control power transmission are shown in Fig.17.

It can be seen from Fig. 17 that the two control strategies can realize bidirectional flow of power under nonlinear load

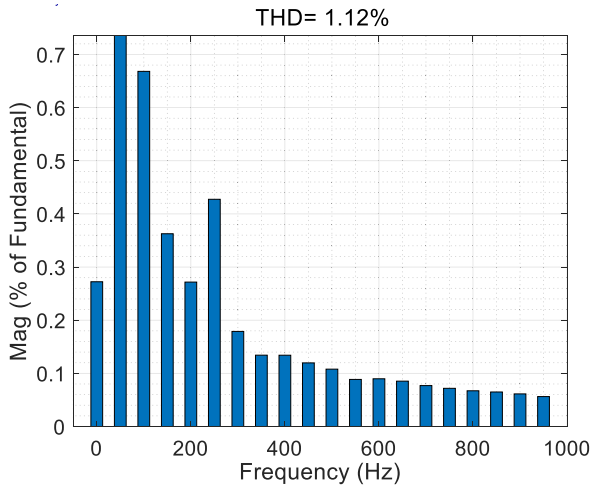

(a) THD of AC side output current in BIC inverter mode.

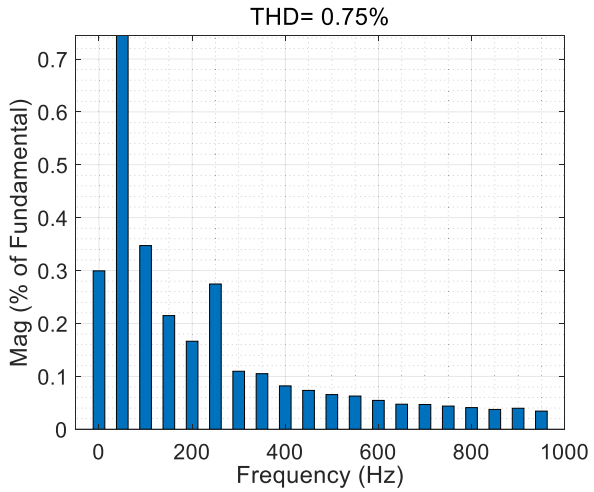

(b) THD of AC side output current in BIC rectifier mode.

FIGURE 18. The BIC AC side output current THD of traditional FDB harmonic suppression control strategy under nonlinear load.

TABLE 3. The main harmonic content after harmonic suppression.

Number	Traditional FBD harmonic suppression droop control strategy		Improved FBD harmonic suppression droop control strategy	
	Inverter mode (%)	Rectifier mode (%)	Inverter mode (%)	Rectifier mode (%)
2	0.67%	0.35%	0.44%	0.18%
3	0.36%	0.21%	0.27%	0.10%
5	0.43%	0.27%	0.29%	0.19%
7	0.13%	0.11%	0.06%	0.07%
9	0.12%	0.07%	0.07%	0.03%
11	0.09%	0.06%	0.07%	0.02%

conditions. Since the two methods are basically consistent in the transmission power diagram. Therefore, the fast Fourier analysis of AC side current of BIC is carried out to make a further comparison from the THD. The simulation results of THD of AC current on the AC side of the BIC by the two methods are shown in Fig. 18 and Fig. 19.

Under the inverter mode of 0.2s∼ 0.2s, the THD of the traditional FBD harmonic suppression control strategy is 1.12%, and the THD of the improved FBD harmonic suppression

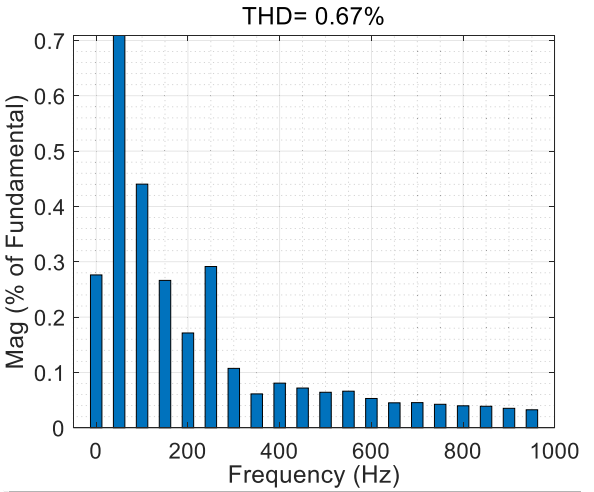

(a) THD of AC side output current in BIC inverter mode.

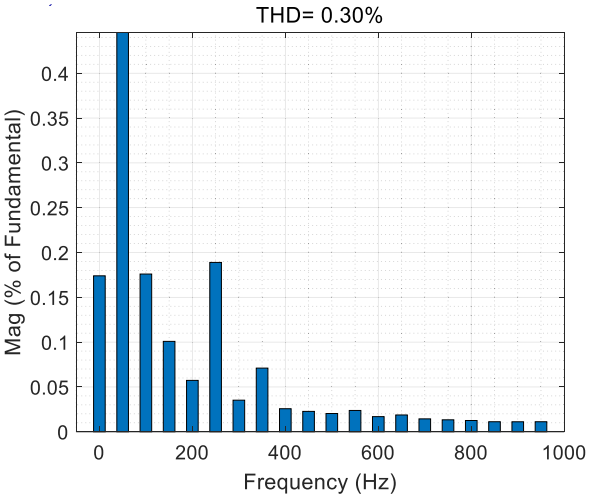

(b) THD of AC side output current in BIC rectifier mode.

FIGURE 19. The BIC AC side output current THD of improved FBD harmonic suppression control strategy under nonlinear load.

control strategy is 0.67%. Under the rectifier mode of 4S ∼6s, the THD of the traditional FBD harmonic suppression control strategy is 0.75%, and the THD of the improved FBD harmonic suppression control strategy is 0.30%. Based on the droop control strategy combined with the two methods of FBD harmonic detection, both the rectifier mode and the inverter mode had THD less than 1%, and the improved control strategy had THD reduced by 0.45%. After adopting the harmonic suppression control strategy, the A-phase current on the AC side of the BIC contains 2nd, 3rd, 5th, 7th, 9th and 11th harmonics, as shown in Table 3.

It can be seen from Table 3 that the harmonic suppression control strategy can effectively suppress the harmonic current component in the BIC and reduce the multiple harmonics content to less than 0.5%. The improved FBD harmonic suppression control strategy has more advantages than the traditional FBD harmonic suppression control strategy, and its THD result is reduced by 0.45% compared with the original method.

V. CONCLUSION

In this article, the traditional FBD harmonic detection method and droop control strategy are analyzed. First of all, the traditional FBD harmonic detection method adopts the traditional PLL, which is unable to achieve accurate phase locking under the non-ideal condition of voltage and current distortion, and the cut-off frequency of the LPF cannot give consideration to the response speed and detection accuracy of the FBD method. Therefore, based on the traditional FBD harmonic current detection method, an improved FBD harmonic current detection method was designed by using DDSRF-PLL and LMS adaptive filters instead of the traditional PLL and LPF. Secondly, only in the droop control strategy, voltage and current distortion will affect the operation of the whole microgrid system under the non-ideal conditions. Therefore, based on the traditional FBD harmonic suppression droop control strategy, an improved FBD harmonic suppression droop control strategy is designed. Finally, through the analysis of simulation results, the improved FBD harmonic suppression droop control strategy can realize the bidirectional flow of power and maintain the stability of DC bus voltage in the grid-connected mode both ideal and non-ideal conditions. Moreover, compared with original control strategy, the improved FBD harmonic suppression control strategy showed that THD was reduced by 0.45% in the non-ideal condition, which proved the effectiveness and feasibility of the method.

In this article, only a single BIC is harmonic suppression control, not in the case of multi-converter analysis, which will be the direction of our future research.

REFERENCES

[1] A. Gupta, S. Doolla, and K. Chatterjee, "Hybrid AC–DC microgrid: Systematic evaluation of control strategies," *IEEE Trans. Smart Grid*, vol. 9, no. 4, pp. 3830–3843, Jul. 2018, doi: 10.1109/TSG.2017.2727344.

[2] C. Ren, L. Liu, X. Han, B. Zhang, L. Wang, and P. Wang, "Multi-mode control for three-phase bidirectional AC/DC converter in hybrid microgrid under unbalanced AC voltage conditions," in *Proc. IEEE Energy Convers. Congr. Expo. (ECCE)*, Baltimore, MD, USA, Sep. 2019, pp. 2658–2663, doi: 10.1109/ECCE.2019.8912259.

[3] F. Nejabatkhah and Y. W. Li, "Overview of power management strategies of hybrid AC/DC microgrid," *IEEE Trans. Power Electron.*, vol. 30, no. 12, pp. 7072–7089, Dec. 2015, doi: 10.1109/TPEL.2014.2384999.

[4] D. Wang, K. Wang, Y. Fei, and Z. Zhang, "Design of static synchronous compensator and its controller based on improved ip-iq detection method," in *Proc. IEEE Sustain. Power Energy Conf. (iSPEC)*, Beijing, China, Nov. 2019, pp. 1038–1041, doi: 10.1109/iSPEC48194.2019.8975134.

[5] T. Su, M. Yang, T. Jin, and R. C. C. Flesch, "Power harmonic and interharmonic detection method in renewable power based on nuttall double-window all-phase FFT algorithm," *IET Renew. Power Gener.*, vol. 12, no. 8, pp. 953–961, Jun. 2018, doi: 10.1049/iet-rpg.2017.0115.

[6] Y. Peng, K. Zhang, Y. Li, P. Yang, and H. Liu, "Improved harmonic detection algorithm applied to APF," in *Proc. 29th Chin. Control Decis. Conf. (CCDC)*, Chongqing, China, May 2017, pp. 6948–6952, doi: 10.1109/CCDC.2017.7978434.

[7] D. Wang, L. Zhang, C. Wang, S. Liu, and Q. Liu, "A harmonic detection strategy based on FBD power theory," in *Proc. IEEE PES Asia–Pacific Power Energy Eng. Conf. (APPEEC)*, Macao, Macao, Dec. 2019, pp. 1–5, doi: 10.1109/APPEEC45492.2019.8994402.

[8] D. C. Raj and D. N. Gaonkar, "Frequency and voltage droop control of parallel inverters in microgrid," in *Proc. 2nd Int. Conf. Control, Instrum., Energy Commun. (CIEC)*, Kolkata, India, Jan. 2016, pp. 407–411, doi: 10.1109/CIEC.2016.7513771.

[9] M. S. Rahman, M. J. Hossain, J. Lu, and H. R. Pota, "A need-based distributed coordination strategy for EV storages in a commercial hybrid AC/DC microgrid with an improved interlinking converter control topology," *IEEE Trans. Energy Convers.*, vol. 33, no. 3, pp. 1372–1383, Sep. 2018, doi: 10.1109/TEC.2017.2784831.

[10] Q. Xu, J. Xiao, P. Wang, and C. Wen, "A decentralized control strategy for economic operation of autonomous AC, DC, and hybrid AC/DC microgrids," *IEEE Trans. Energy Convers.*, vol. 32, no. 4, pp. 1345–1355, Dec. 2017, doi: 10.1109/TEC.2017.2696979.

[11] Z. Gao, C. Li, W. Teng, C. Tian, and Y. Rao, "Hybrid microgrid load distribution and DC voltage control," in *Proc. IEEE 3rd Conf. Energy Internet Energy Syst. Integr. (EI2)*, Changsha, China, Nov. 2019, pp. 1933–1937, doi: 10.1109/EI247390.2019.9062240.

[12] Y. Q. Zhu, Q. Zhang, K. Liu, Z. Wang, and F. Y. Wang, "Segmented coordination control strategy for hybrid AC/DC microgrid," *Autom. Electric Power Syst.*, vol. 44, no. 6, pp. 52–58, 2020.

[13] X. Yang, F. Tang, X. Wu, and X. Jin, "Hierarchical control strategy of grid-connected DC microgrids," in *Proc. IEEE 8th Int. Power Electron. Motion Control Conf. (IPEMC-ECCE Asia)*, May 2016, pp. 3723–3727, doi: 10.1109/IPEMC.2016.7512891.

[14] D. Phan and H. Lee, "Interlinking converter to improve power quality in hybrid AC–DC microgrids with nonlinear loads," *IEEE J. Emerg. Sel. Topics Power Electron.*, vol. 7, no. 3, pp. 1959–1968, Sep. 2019, doi: 10.1109/JESTPE.2018.2870741.

[15] P. Goleij, S. HajiAghasi, and A. Salemnia, "A new hybridization concept for distributed generation and microgrids under harmonic and nonlinear loads," in *Proc. Smart Grid Conf. (SGC)*, Sanandaj, Iran, Nov. 2018, pp. 1–6, doi: 10.1109/SGC.2018.8777778.

[16] H. Tian, X. H. Wen, and Y. W. Li, "A harmonic compensation approach for interlinking voltage source converters in hybrid AC-DC microgrids with low switching frequency," *CSEE J. Power Energy Syst.*, vol. 4, no. 1, pp. 39–48, Mar. 2018.

[17] Q. Liu and Y. Li, "An inductive filtering-based parallel operating transformer with shared filter for power quality improvement of wind farm," *IEEE Trans. Power Electron.*, vol. 35, no. 9, pp. 9281–9290, Sep. 2020, doi: 10.1109/TPEL.2020.2973702.

[18] T. Dinesh Patil and D. S. More, "Comparative analysis of cuk converter with proportional integral controller & proportional resonant controller," in *Proc. Int. Conf. Commun. Electron. Syst. (ICCES)*, Coimbatore, India, Jul. 2019, pp. 1654–1659, doi: 10.1109/ICCES45898.2019.9002320.

[19] Q. Liu, Y. Li, S. Hu, and L. Luo, "Power quality improvement using controllable inductive power filtering method for industrial DC supply system," *Control Eng. Pract.*, vol. 83, pp. 1–10, Feb. 2019.

[20] L. F. Liu, X. Q. Han, C. G. Ren, P. Wang, B. F. Zhang, and S. W. Li, "Multimode operation control scheme for AC/DC interfacing converter under unbalance conditions in hybrid microgrid," *Gaodianya Jishu*, vol. 45, pp. 4003–4012, 2019.

[21] H. R. Baghaee, M. Mirsalim, G. B. Gharehpetan, and H. A. Talebi, "Nonlinear load sharing and voltage compensation of microgrids based on harmonic power-flow calculations using radial basis function neural networks," *IEEE Syst. J.*, vol. 12, no. 3, pp. 2749–2759, Sep. 2018, doi: 10.1109/JSYST.2016.2645165.

[22] S. Dahale and T. Hinge, "Harmonics reduction in microgrids using APF with fuzzy controller," in *Proc. Innov. Power Adv. Comput. Technol. (i-PACT)*, Vellore, India, Mar. 2019, pp. 1–6, doi: 10.1109/i-PACT44901.2019.8960029.

[23] S. Li, J. Wang, T. Wang, H. Du, Y. Duan, H. Gao, R. Meng, L. Wang, X. Han, M. Wei, B. Zhao, P. Wang, L. H. Koh, and J. Xiao, "The bidirectional AC/DC power converter with capability of suppressing the harmonic current in hybrid micro grid," in *Proc. Asian Conf. Energy, Power Transp. Electrific. (ACEPT)*, Singapore, Oct. 2018, pp. 1–6, doi: 10.1109/ACEPT.2018.8610667.

[24] P. Lin, C. Jin, J. Xiao, X. Li, D. Shi, Y. Tang, and P. Wang, "A distributed control architecture for global system economic operation in autonomous hybrid AC/DC microgrids," *IEEE Trans. Smart Grid*, vol. 10, no. 3, pp. 2603–2617, May 2019, doi: 10.1109/TSG.2018.2805839.

[25] B. Liang, L. Kang, J. He, F. Zheng, Y. Xia, Z. Zhang, Z. Zhang, G. Liu, and Y. Zhao, "Coordination control of hybrid AC/DC microgrid," *J. Eng.*, vol. 2019, no. 16, pp. 3264–3269, Mar. 2019, doi: 10.1049/joe.2018.8505.

[26] Z. W. Liu, S. H. Miao, Z. H. Fan, Y. L. Kang, K. Y. Chao, and D. D. Sun, "Power control and voltage fluctuation suppression strategy of the bidirectional AC/DC converter in the Islanding hybrid microgrid," *Proc. Chin. Soc. Electr. Eng.*, vol. 39, no. 21, pp. 6225–6237, 2019.

[27] W. Hu, H. Chen, X. Yang, K. Xu, and P. Hu, "Control strategy of the bi-directional converter for hybrid AC/DC microgrid," in *Proc. IEEE PES Asia–Pacific Power Energy Eng. Conf. (APPEEC)*, Brisbane, QLD, Australia, Nov. 2015, pp. 1–5, doi: 10.1109/APPEEC.2015.7380923.
[28] M. Xiaochun, W. Xiaohong, L. Yang, S. Shouxin, and Z. Chao, "Research on improvement of voltage fluctuation in micro-grid based on improved double closed loop control of flywheel battery," in *Proc. IEEE 3rd Adv. Inf. Manage., Communicates, Electron. Autom. Control Conf. (IMCEC)*, Chongqing, China, Oct. 2019, pp. 1876–1880, doi: 10.1109/IMCEC46724.2019.8984010.
[29] Z. Han, X. L. Wang, B. C. Jiang, and J. R. Chen, "A control strategy for suppressing zero-sequence circulating current in paralleled three-phase voltage-source PWM converters," *Appl. Sci.*, vol. 10, no. 5, p. 1703, 2020.
[30] L. Liu, D. Xie, D. Zhao, Y. Jia, Y. Yu, Q. Fan, Y. Shen, and W. Qi, "Harmonic current detection and reactive power compensation method for photovoltaic system based on FBD method," in *Proc. IEEE 3rd Conf. Energy Internet Energy Syst. Integr. (EI2)*, Changsha, China, Nov. 2019, pp. 1970–1975, doi: 10.1109/EI247390.2019.9062008.
[31] X. Q. Wu, Y. C. Wang, X. Chen, J. Chen, G. Q. He, and G. H. Li, "Sequence impedance model and interaction stability research of three-phase grid-connected inverters with considering coupling effects," *Proc. Chin. Soc. Electr. Eng.*, vol. 40, no. 5, pp. 1605–1616, Mar. 2020.
[32] A. Ghasemi, M. H. Refan, and P. Amiri, "An implementation of improved PLL for control of grid-connected converters under grid perturbations," *J. Control, Automat. Elect. Syst.*, vol. 30, no. 4, pp. 568–579, Aug. 2019.
[33] J. Z. Zhang, Z. Geng, S. Xu, and H. Chen, "An improved adaptive harmonic detection algorithm for active power filter," *Trans. China Electrotech. Soc.*, vol. 34, no. 20, pp. 4323–4333, Oct. 2019.

GUISHUO WANG (Fellow, IEEE) is currently with the School of Mechanical, Electrical and Information Engineering, Shandong University, Weihai, China.

He received the B.S. degree in communication engineering from Taishan University, Tai'an, China, in 2017. He is currently pursuing the M.E. degree in electronics and communications engineering with Shandong University. His current research interests include ac–dc hybrid microgrid, interlinking converter, and control strategy.

XIAOLI WANG (Fellow, IEEE) is currently with the School of Mechanical, Electrical and Information Engineering, Shandong University, Weihai, China.

He received the B.E. degree in electronic science and technology and the M.E. degree in circuits and systems from Shandong University. He is currently a Senior Experimentalist and a Supervisor of master's student with Shandong University. His current research interests include ac–dc hybrid microgrid, smart grid, and the Internet of Things wireless communication.

JIECHAO LV is currently with the School of Mechanical, Electrical and Information Engineering, Shandong University, Weihai, China.

He received the B.S. degree in communication engineering from Qingdao University, Qingdao, China, in 2018. He is currently pursuing the M.E. degree in electronics and communications engineering with Shandong University. His current research interests include ac–dc hybrid microgrid and energy storage systems.